Models of synthetic aperture radar backscattering for bright flows and dark spots on Titan

Philippe Paillou,[1] Marc Crapeau,[1] Charles Elachi,[2] Stephen Wall,[2] and Pierre Encrenaz[3]

Received 29 March 2006; revised 10 July 2006; accepted 12 July 2006; published 25 November 2006.

[1] The synthetic aperture radar (SAR) imaging mode of the Cassini RADAR instrument enables us to map the surface of Titan through its thick atmosphere. The first Cassini close flyby, acquired on 26 October 2004, revealed a complex surface, with areas of low relief and dome-like volcanic constructs, flows, and sinuous channels. In particular, fan-like features with strong radar backscattering were observed. Such structures, extending from tens of kilometers to more than 200 km in length, could be the result of cryovolcanism. Several radar dark spots, up to 30 km across, were also observed; they may correspond to smooth hydrocarbon deposits. We present here a first modeling of these radar-bright and radar-dark features on the basis of classical radar backscattering models. We considered two main materials which could constitute the surface of Titan, tholins and water-ammonia ice, and modeled both single- and two-layer cases, taking into account volume and subsurface scattering. Our results show that SAR-bright regions could better be explained by the effect of a thin layer of water-ammonia ice covering a tholin substratum. Radar-dark spots can be modeled in two ways: a rough tholin surface or a smooth one with some volume scattering. We show that multi-incidence SAR data could help discriminate between the various scenarios proposed.

Citation: Paillou, P., M. Crapeau, C. Elachi, S. Wall, and P. Encrenaz (2006), Models of synthetic aperture radar backscattering for bright flows and dark spots on Titan, *J. Geophys. Res.*, *111*, E11011, doi:10.1029/2006JE002724.

1. Introduction

[2] The study of Titan, the only moon in the solar System to host a thick atmosphere, is one major scientific objective of the Cassini-Huygens mission which reached Saturn in July 2004. Several flybys over Titan have been made up to now (more than 40 are planned), allowing various instruments onboard the Cassini orbiter to study the atmosphere and the surface of the satellite. Among them, the Cassini RADAR instrument [*Elachi et al.*, 2004] is able to "see" Titan's surface through its permanent and thick atmosphere, since microwaves are not diffused by atmospheric particles as it was successfully demonstrated with the Magellan mission at Venus [*Saunders et al.*, 1992]. RADAR is a high-frequency Ku band (13.8 GHz, 2.18 cm) radar, operating in four modes: radiometry, scatterometry, altimetry and synthetic aperture radar (SAR) imaging. The SAR mode allows us to reveal the surface of Titan with a high resolution better than 500 m/pixel.

[3] The first Cassini close flyby of Titan (Ta) was realized on 26 October 2004, at a minimum range of 1174 km. The SAR image strip acquired during this flyby covers about 100° in longitude and it revealed a complex surface, with areas of low relief and dome-like volcanic constructs, flows and sinuous channels [*Elachi et al.*, 2005]. In particular, channels and fan-like features with a strong radar backscattering were observed: such strong SAR signal could be explained by a high component of volume scattering [*Paganelli et al.*, 2005]. Fan-like features, extending from tens of kilometers to more than 200 km in length, could be flowing material resulting from cryovolcanism [*Sotin et al.*, 2005] related to a large circular feature about 180 km in diameter located 49.7°N, 87.3°W [*Lopes et al.*, 2005]. Also, a number of isolated radar-dark spots, up to 30 km across, were observed. They could correspond to smooth liquid hydrocarbon deposits [*Lorenz et al.*, 2005].

[4] We present here a first analysis of some of the radar-bright and radar-dark features observed in the SAR data of the Ta flyby. We used classical SAR backscattering models and considered two main materials which could constitute the surface of Titan: tholins and water-ammonia ice. We modeled both the single and two-layer cases, taking into account volume and subsurface scattering. A two-layer scenario allows to reproduce the strong radar backscattering observed in SAR-bright regions with a reasonably low volume scattering component, while the radar signature of dark spots can be modeled using both rough and smooth surface conditions. We show that the SAR data with different incidence angles that will be acquired in the

[1] UMR 5804, Observatoire Aquitain des Sciences de l'Univers, Floirac, France.
[2] Jet Propulsion Laboratory, Pasadena, California, USA.
[3] Laboratorie d'Etude du Rayonnement et de la Matiére en Astrophysique, Observatoire de Paris, Paris, France.

0148-0227/06/2006JE002724

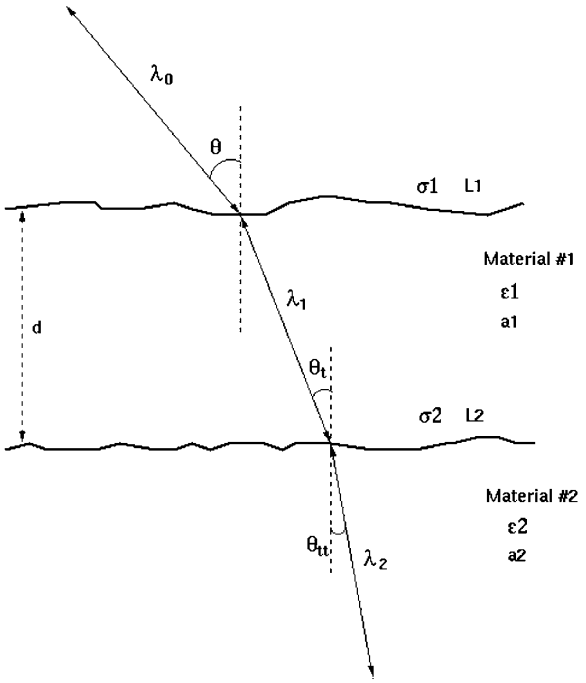

Figure 1. Sketch of the two-layer model of Titan's subsurface with relevant parameters.

future could help discriminate between the various models proposed.

2. SAR Modeling

[5] We shall consider in the following that the "radar-dark" and "radar-gray" material observed in Cassini SAR images could be representative of the global tholin-composed surface of Titan [*Lunine*, 1993]. Dielectric constant of tholins is estimated to $\varepsilon = 2.2-0.01i$ [*Rodriguez et al.*, 2003] within the 2–3 range obtained from the radiometry mode [*Elachi et al.*, 2005] (the dielectric constant estimated from the radiometer represents a mean value for the entire visible disk of Titan, but considerable brightness temperature variations can be observed locally). If of cryovolcanic origin, SAR-bright flows could be composed of a mixture of water ice and ammonia, whose dielectric constant is estimated to be $\varepsilon = 4.5-0.04i$ [*Lorenz et al.*, 2003]. The penetration capabilities of a Ku band SAR in Titan's subsurface can then be estimated using the relationship [*Ulaby et al.*, 1982]

$$\delta_P = \frac{\lambda_0}{4\pi}\left\{\frac{\varepsilon'}{2}\left[\sqrt{1+\left(\frac{\varepsilon''}{\varepsilon'}\right)^2}-1\right]\right\}^{-1/2} \quad (1)$$

At Ku band ($\lambda_0 = 2.18$ cm), a SAR should penetrate around 0.5 m in tholins ($\varepsilon = 2.2-0.01i$) and 0.2 m in a water ice/ammonia mixture ($\varepsilon = 4.5-0.04i$). The penetration depth of Ku band in Titan's subsurface is then likely to be less than half a meter. Such a low penetration depth hardly allows to consider volume or coherent scattering as an explanation for very high radar reflectivity, as it was done for Europa for instance [*Ostro et al.*, 1992]: Earth-based radar observations at centimeter wavelength have shown that Europa radar albedo is higher that the one recorded for comets, nonmetallic asteroids, the Moon and the inner planets. This was explained as the result of constructive interferences in the radar backscattering along the wave path: it requires closely spaced scattering heterogeneities of the wavelength size, in a transparent medium allowing several meters of penetration depth. High radar reflectivity was also observed on Earth over the Greenland Ice Sheet [*Rignot*, 1995]. This phenomenon is caused by enhanced scattering from massive and large solid ice bodies buried in the top few meters of the dry and cold snowy surface. Again, this requires several meters of penetration depth in a very transparent medium.

[6] Even if such a medium (pure, dry and cold water ice) could exist on the surface of Titan, we chose here to study the radar response of a two-layer surface to propose an explanation for SAR-bright regions, taking into account the low penetration capability of Ku band. We considered the two-layer model in Figure 1 to describe the first meter of Titan's subsurface: a superficial layer of material 1, of thickness d, covers a subsurface layer of material 2. The first layer is characterized by its dielectric constant (real part ε'_1 and imaginary part ε''_1), its surface roughness (height standard deviation σ_1, correlation length L_1, autocorrelation function taken as Gaussian) and its albedo a_1 (the ratio between the extinction coefficient κ_e and the diffusion coefficient κ_s). The second layer is also characterized by its roughness (height standard deviation σ_2, correlation length L_2, autocorrelation function taken as Gaussian), dielectric constant (real part ε'_2 and imaginary part ε''_2) and its albedo a_2. This two-layer model is illuminated by a radar wave of wavelength λ_0 arriving with an incidence angle θ. It should be noted that the radar wavelength changes when propagating into materials 1 and 2, together with its incidence angle.

[7] In order to take into account various surface roughness conditions (from very smooth to very rough surfaces compared to the radar wavelength), we had to deal with different backscattering models: integral equation model (IEM) [*Fung et al.*, 1992], physical optics (PO) model [*Ulaby et al.*, 1982], and geometric optics (GO) model [*Fung and Eom*, 1981]. IEM concerns smooth to medium-rough surfaces, while PO and GO models are adapted to rough surfaces. At Ku band, a surface can be considered rough for $\sigma > 1$ cm and $L > 2$ cm.

2.1. Integral Equation Model (Smooth to Medium-Rough Surfaces)

[8] The domain of validity of the IEM model can be defined by the relationships

$$k\sigma < 3 \qquad k\sigma kL < 1.5\sqrt{|\varepsilon|} \quad (2)$$

where σ and L describe the roughness of a surface of dielectric constant ε, illuminated by a radar wave of wave number $k = 2\pi/\lambda$. The surface radar backscattering coefficient can be expressed by

$$\sigma^0_{Spp}(\theta) = \frac{k}{4}e^{-2k^2\cos^2(\theta)\sigma^2}\sum_{n=1}^{\infty}\left|I^n_{pp}\right|^2\frac{W^{(n)}(-2k\sin(\theta),0)}{n!} \quad (3)$$

with

$$I_{pp}^{n} = (2k\cos(\theta)\sigma)^{n} f_{pp} e^{-k^2\cos^2(\theta)\sigma^2} + \frac{(k\cos(\theta)\sigma)^{n}}{2}\left[F_{pp}(-k\sin(\theta)) + F_{pp}(k\sin(\theta))\right] \quad (4)$$

and

$$W^{(n)}(u,v) = \sqrt{\frac{\pi}{n}} L e^{-\frac{(u+v)^2 L^2}{4n}} \quad (5)$$

being the Fourier transform of the nth power of the surface correlation function, that we considered Gaussian, and f_{pp} and F_{pp} being respectively the coefficient of the Kirchoff fields and complementary fields [*Fung*, 1994].

2.2. Physical Optics Model (Medium-Rough to Rough Surfaces)

[9] The PO model validity range is defined by the following conditions:

$$kL > 6 \qquad \frac{1}{k} < \sigma < 0.06kL^2 \quad (6)$$

where k is the wave number of the incident plane wave. The noncoherent surface scattering coefficient is then given as a function of the incidence angle θ by [*Ulaby et al.*, 1982]

$$\sigma_{Spp}^{0}(\theta) = 2k^2\cos^2\theta\,\Gamma_{pp}(\theta) e^{-(2k\sigma\cos\theta)^2} \cdot \sum_{n=1}^{\infty}\left(4k^2\sigma^2\cos^2\theta\right)^{n}/n! \int_{0}^{\infty}\rho^{n}(x) J_0(2kx\sin\theta) x dx \quad (7)$$

where J_0 is the zeroth-order Bessel function of the first kind, $\Gamma_{pp}(\theta) = |R_{pp}(\theta)|^2$ is the Fresnel reflectivity, and $\rho(x) = \exp(-x^2/L^2)$ is the Gaussian surface autocorrelation function.

2.3. Geometrical Optics Model (Very Rough Surfaces)

[10] The GO model validity range is expressed by

$$(2k\sigma\cos\theta)^2 > 10 \quad \text{and} \quad kL > 6 \quad (8)$$

and the noncoherent surface scattering term is given as a function of the incidence angle θ by [*Fung and Eom*, 1981]:

$$\sigma_{Spp}^{0} = \frac{\Gamma(0) e^{-\tan^2(\theta)/2m^2}}{2m^2\cos^4\theta} \quad (9)$$

where $m = \sqrt{2}\sigma/L$ is the RMS slope for a Gaussian surface, and $\Gamma(0)$ is the Fresnel reflectivity evaluated at normal incidence:

$$\Gamma(0) = \left|\frac{1-\sqrt{\varepsilon}}{1+\sqrt{\varepsilon}}\right|^2 \quad (10)$$

2.4. Volume Scattering Term

[11] We also have to take into account a volume scattering term which should be added to the surface scattering term, in order to simulate the diffusion effects of heterogeneities in materials. The volume scattering component does not depend on roughness parameters, it mainly changes with the albedo a and optical depth τ of the material:

$$\sigma_{Vpp}^{0}(\theta) = \frac{1}{2} a T_{12} T_{21}\cos(\theta)\left(1 - e^{-\frac{2\tau}{\cos(\theta_t)}}\right) P_{pp} \quad (11)$$

where T_{ij} is the Fresnel transmission coefficient from medium i to medium j and P_{pp} has a value 1.5 [*Fung*, 1994]. When scattering in the material is low, *Ulaby et al.* [1982] gives the relationships between the extinction coefficient κ_e, the scattering coefficient κ_s, the absorption coefficient κ_a, the albedo a and the penetration depth δ_p:

$$\kappa_e = \kappa_a + \kappa_s \qquad a = \frac{\kappa_s}{\kappa_e} \qquad \kappa_a = \frac{1}{\delta_p} \quad (12)$$

We can then define a convenient optical depth τ using the albedo a only:

$$\tau = \kappa_e \delta_p = \frac{1}{1-a} \quad (13)$$

2.5. Subsurface Scattering Term

[12] We also have to compute a subsurface component, which is the surface scattering term of the second layer attenuated by its propagation through the first layer:

$$\sigma_{SSpp}^{0}(\theta) = \frac{\cos(\theta)}{\cos(\theta_t)} T_{12} T_{21} e^{-\frac{2\tau}{\cos(\theta_t)}} \sigma_{Spp}^{0}(\theta_t) \quad (14)$$

where σ_{Spp}^{0} is obtained from equations (3), (7) or (9) for the second layer of parameters ε_2, σ_2 and L_2, and θ_t is the angle between the transmitted radar wave into the first layer and the normal to the surface.

3. Radar-Bright Regions

[13] We studied the SAR image extract presented in Figure 2. We considered two regions: region 1 is characterized by a rather low SAR backscattering typical of a radar-gray homogeneous unit [*Elachi et al.*, 2005], while region 2 corresponds to SAR-bright fan-like features which could be related to flowing material covering the radar-gray unit. SAR illumination is from the left and the terrain is supposed to be rather flat. The studied region is located around coordinates 50.92°N, 79.35°W, and the SAR incidence angle there is close to 30°. We worked on SAR normalized cross-section values (σ^0), not corrected for incidence angle effect, at a projected resolution of 175 m per pixel: region 1 presents an average backscattered power of −7.5 dB, while region 2 corresponds to a σ^0 value around 0 dB.

3.1. Modeling Results

[14] We compared two models which can both reproduce the measured backscattered power for SAR-bright features

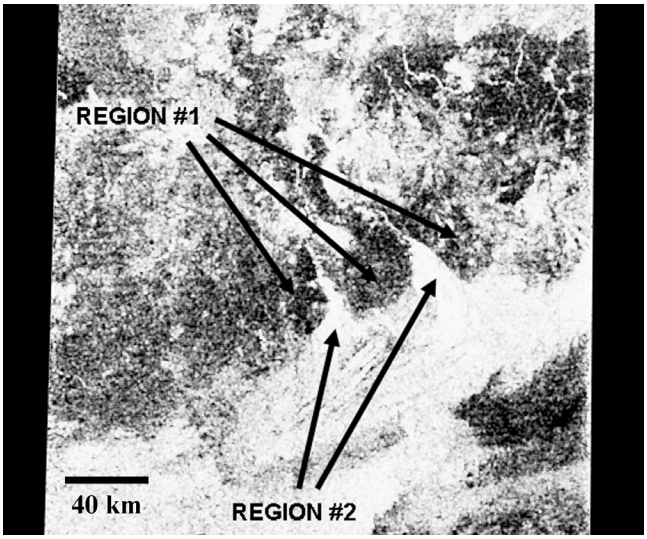

Figure 2. Radar-bright study site located at 50.92°N, 79.35°W.

of region 2: a one-layer model which needs a strong volume scattering component, and a two-layer model which allows us to deal with low albedo values.

3.1.1. One-Layer Model

[15] In the one-layer case, the total backscattered power is the sum of a surface contribution σ^0_{Spp}, obtained from equations (3), (7) or (9), and a volume contribution σ^0_{Vpp} obtained from equation (11):

$$\sigma^0 = \sigma^0_{Spp} + \sigma^0_{Vpp} \tag{15}$$

[16] First, we computed the surface scattering component for both tholins ($\varepsilon = 2.2-0.01i$) and water ice/ammonia mixture ($\varepsilon = 4.5-0.04i$) at an incidence angle $\theta = 30°$ with varying surface roughness parameters: $0 < \sigma < 2$ cm and $0 < L < 4$ cm. Results for tholins are shown on Figure 3, both materials behave the same way.

[17] For tholins, a maximum backscattered power of -8.28 dB is reached for the roughness parameter values $\sigma = 0.65$ cm and $L = 2.25$ cm. Clearly, some volume scattering contribution is still needed to reach the observed σ^0 value -7.5 dB for radar-gray region 1, if composed of tholin-like materials. For a low albedo value $a = 0.02$, the volume scattering term in (11) is -16.56 dB, which added to the surface term yields a total backscattered power of -7.68 dB. Of course, a similar result can be obtained with a lower surface component associated with a higher volume scattering. However, a very high volume scattering effect is not required to explain for the SAR response of region 1.

[18] The maximum backscattered power for a water ice/ammonia mixture is obtained for $\sigma = 1.10$ cm and $L = 3.80$ cm and is not higher than -2.95 dB, i.e., still far from the observed 0 dB of radar-bright region 2. Such a strong σ^0 value cannot be reached considering only the surface scattering term. We have to add a significant volume scattering term, corresponding to a high albedo value: taking $a = 0.5$ in (11) and computing (15) produces a total backscattered power of 0.26 dB for region 2. In this latter case, the volume scattering term is -2.55 dB, i.e., higher than the surface scattering term. Such high values of albedo are not easy to obtain in natural materials. Considering a water ice/ammonia mixture with a penetration depth $\delta_p = 0.2$ m obtained from (1) and an albedo value $a = 0.5$, using (12) allows one to compute an extinction coefficient $\kappa_e = 10$. This is higher than extinction coefficients measured for various snow types on Earth (cf. measurements at 18 GHz by *Hallikainen et al.* [1987]). Also, in the hypothesis of a highly porous cryovolcanic flow for instance [*Paganelli et al.*, 2005], the gas content of pores would reduce the global dielectric constant of the material (i.e., a permittivity lower than 4.5), needing even higher albedo values to reach the observed backscattered power.

3.1.2. Two-Layer Model

[19] Another possibility to model radar-bright flows is to consider a two-layer model. *Elachi et al.* [1984] have shown that surface scattering can be enhanced by the presence of a thin superficial layer which lowers the radar incidence angle. For instance, a Ku band radar wave arriving with an incidence angle of $\theta = 30°$ on a water-ammonia ice layer of dielectric constant $\varepsilon = 4.5-0.04i$ is transmitted to the subsurface with an angle $\theta_t = 13.6°$, its wavelength decreasing to $\lambda_1 = 1.03$ cm. We considered the two-layer model presented in Figure 1, where a thin water-ammonia ice layer covers a tholin substratum. For $\theta_t = 13.6°$, a maximum surface scattering of -2.73 dB can be obtained for a subsurface tholin layer of roughness parameters $\sigma = 0.40$ cm and $L = 3.30$ cm.

[20] In order to obtain the total backscattered power for the two-layer configuration, we have to compute the sum

$$\sigma^0 = \sigma^0_{1Spp} + \sigma^0_{1Vpp} + \sigma^0_{2SSpp} + \sigma^0_{2Vpp} \tag{16}$$

where σ^0_{1Spp} is the surface contribution of the first layer obtained from equations (3), (7) or (9), σ^0_{1Vpp} is the volume contribution of the first layer obtained from equation (11), σ^0_{2SSpp} is the subsurface contribution of the second layer obtained from equation (14), and σ^0_{2Vpp} is the volume contribution of the second layer attenuated by the first layer.

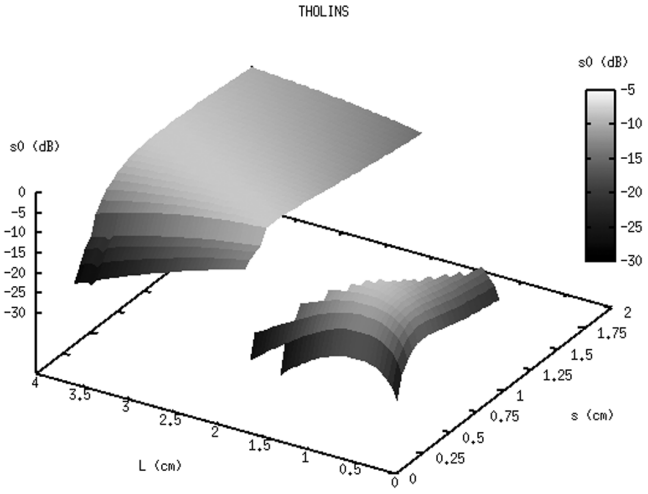

Figure 3. Backscattered power of a single layer of tholins with respect to roughness parameters σ and L at an incidence angle $\theta = 30°$.

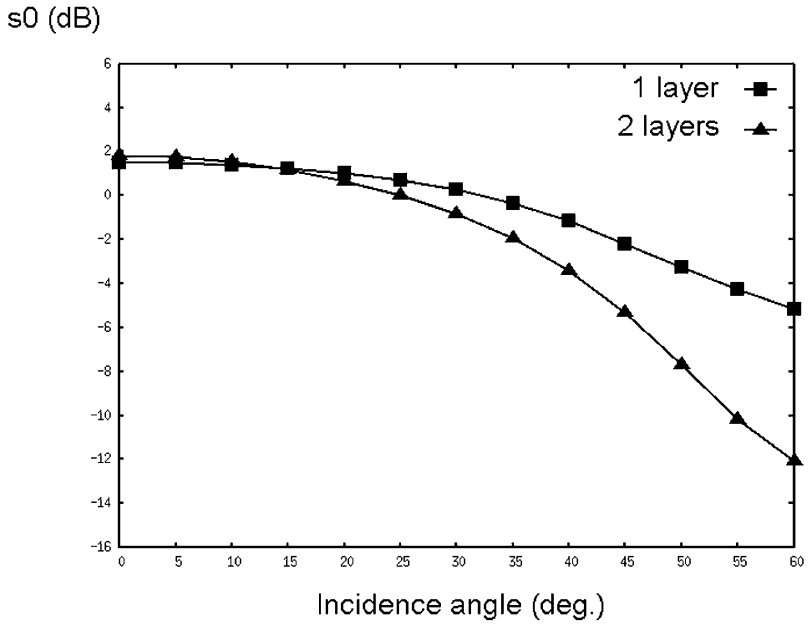

Figure 4. One-layer (squares) and two-layer (triangles) backscattering power of radar-bright regions with respect to the SAR incidence angle.

[21] We then considered a two-layer problem described as follows: a thin water-ammonia ice layer ($\varepsilon_1 = 4.5-0.04i$, cf. material 1 in Figure 1) of thickness $d = 5$ cm and roughness parameters $\sigma_1 = 1.10$ cm and $L_1 = 3.80$ cm, of very low albedo value $a_1 = 0.01$, covering a tholin layer ($\varepsilon_2 = 2.2-0.01i$, cf. material 2 in Figure 1) of roughness parameters $\sigma_2 = 0.40$ cm and $L_2 = 3.30$ cm with a reasonable albedo value $a_2 = 0.15$. We obtain from (16) a total backscattered power $\sigma^0 = -0.83$ dB, corresponding to $\sigma^0_{1Spp} = -2.95$ dB, $\sigma^0_{1Vpp} = -29.57$ dB, $\sigma^0_{2SSpp} = -6.32$ dB and $\sigma^0_{2Vpp} = -10.76$ dB. The σ^0 value obtained is closed to the observed one for SAR-bright flows, which could then be easily described as a thin layer of water-ammonia ice covering tholins without the need for a high volume scattering component.

3.2. Using Multi-Incidence Data

[22] SAR data available from Ta flyby are not sufficient to discriminate between the one-layer and two-layer hypotheses for SAR-bright regions, since both models can reproduce the observed backscattered power. A solution to favor one hypothesis would be to acquire Ku band SAR images of the same region with a different incidence angle.

[23] Figure 4 shows the computed "one-layer" (squares) and "two-layer" (triangles) σ^0 value of radar-bright flows at various incidence angles. As the one-layer hypothesis relies on a strong volume scattering component, it presents a rather diffuse behavior; that is, σ^0 slowly decreases as the incidence angle increases. On the contrary, the two-layer model is closer to the pure surface scattering case, and then σ^0 decreases faster as the incidence angle increases.

[24] For instance, for $\theta = 45°$, $\sigma^0 = -2.18$ dB for the one-layer case whereas $\sigma^0 = -5.32$ dB for the two-layer case. So, higher incidence SAR images of radar-bright flows could help discriminating between the two hypotheses and then contribute to better understand possible cryovolcanic processes on Titan.

4. Radar-Dark Spots

[25] We also tried to model the SAR response of isolated radar-dark spots. Figure 5 shows such structures observed during the Ta flyby. These regions are much darker than the rest of the SAR image strip, with a backscattered power ranging between −13 dB and −10 dB, still about 5 dB higher than the SAR noise level. Both are roughly circular of diameter around 20 km. Radar-dark spot A (Figure 5, left) is located at 51.23°N, 76.53°W and corresponds to a SAR incidence angle close to 30°, while radar-dark spot B (Figure 5, right) is located at 49.48°N, 69.73°W and corresponds to a SAR incidence angle close to 23°. Passive radiometry data show that dark spots are 3 K higher in brightness temperature than their surroundings, which corresponds to a rather high emissivity, consistent with a dielectric constant around 2. Radar-dark spots were inter-

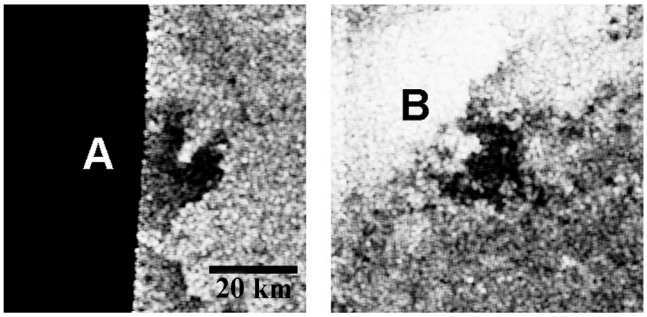

Figure 5. Radar-dark spots (left) A at incidence angle 30° and (right) B at incidence angle 23° in Ta flyby SAR data.

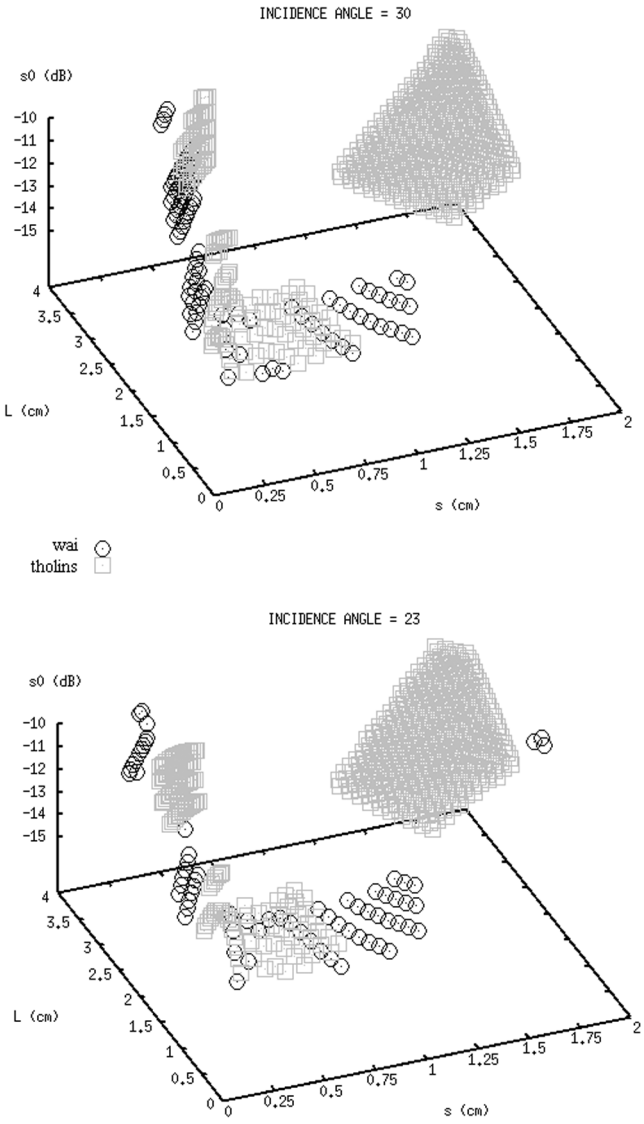

Figure 6. Backscattered power for a single layer of tholins (gray squares) and water-ammonia ice (black circles) with respect to roughness parameters σ and L at incidence angle (top) $\theta = 30°$ and (bottom) $\theta = 23°$.

preted as possible smooth liquid hydrocarbon deposits or impact remains [*Lorenz et al.*, 2005].

4.1. Modeling Results

[26] The low backscattered power of radar-dark spots can be easily reproduced using a simple one-layer surface scattering model, without any volume scattering component. We considered surface scattering expressions given by (3), (7) and (9), for both tholins ($\varepsilon = 2.2-0.01i$) and water-ammonia ice ($\varepsilon = 4.5-0.04i$), with varying surface roughness parameters: $0 < \sigma < 2$ cm and $0 < L < 4$ cm. Results are shown on Figure 6, for both incidence angles $\theta = 30°$ and $\theta = 23°$. We kept the computed backscattered power between -13 dB and -10 dB, corresponding to the observed σ^0 for radar-dark spots.

[27] One can see that few (σ, L) combinations of roughness parameters for the water-ammonia ice case are able to produce σ^0 values in the observed range (cf. black circles in Figure 6), while large regions of the roughness parameter plane fall into the right σ_0 range for tholins (cf. gray squares in Figure 6). For both incidence angles, a rough tholin surface with roughness parameters $1 < \sigma < 2$ cm and $2 < L < 4$ cm can easily produce a backscattered power in the -13 dB/-10 dB range.

[28] So, a rough tholin-covered surface could be responsible for radar-dark spots, although smoother surfaces with some volume scattering contribution can also produce the same result. For instance, at an incidence angle $\theta = 30°$, a rough tholin surface of roughness parameters $\sigma = 1.50$ cm and $L = 2.50$ cm with a zero albedo value produces a backscattered power $\sigma^0 = -11.30$ dB, (GO model domain, cf. (9)), while a smooth tholin surface of roughness parameters $\sigma = 0.10$ cm and $L = 1.00$ cm but with a low albedo value $a = 0.05$ produces a total backscattered power $\sigma^0 = -11.47$ dB. The surface scattering component in this latter case is -18.08 dB (IEM domain, cf. (3)) and the volume scattering component is -12.54 dB (cf. (11)).

4.2. Using Multi-Incidence Data

[29] Again, as for radar-bright regions, using multi-incidence SAR data of the same radar-dark spot could help discriminate between the "smooth" and "rough" scenario. Figure 7 shows the computed "surface scattering only" (squares) and "surface plus volume scattering" (triangles) σ^0 values for a radar-dark spot made of tholins, at various incidence angles. Both models produce the same backscattered power for the incidence angle $\theta = 30°$, but the "surface only" model considers a rough surface ($\sigma = 1.50$ cm and $L = 2.50$ cm, GO model used), while the "surface plus volume" model relies on a smoother surface ($\sigma = 0.10$ cm and $L = 1.00$ cm, IEM used) with a low volume scattering term of albedo $a = 0.05$.

[30] As a result, one can see that σ^0 slowly increases with the incidence angle for a rough surface (squares), whereas it decreases as the incidence angle increases for a smoother surface (triangles). For instance, at a low incidence angle $\theta = 10°$, $\sigma^0 = -8.37$ dB for the smooth surface plus volume scattering case whereas $\sigma^0 = -12.62$ dB for the rough surface case. Thus low-incidence SAR images of radar-dark spots could discriminate between a rough and a smooth surface, and then help validate the hypothesis of hydrocarbon lakes for instance.

5. Conclusion

[31] We used classical electromagnetic models of radar scattering in order to study SAR-bright and dark features observed on the Titan's surface during the Cassini Ta flyby. First interpretations of our model results show that SAR-bright regions, possibly corresponding to flowing material resulting from cryovolcanism, can be explained by both strong volume scattering in a thick water-ammonia ice layer and by the effect of a thin layer of such material covering a tholin substratum. The latter hypothesis is favored since it requires a lower volume scattering effect, consistent with low penetration capabilities of Ku band. If confirmed, it could help understand processes which transfer material from the subsurface to the surface of Titan, such as episodic outgassing [*Tobie et al.*, 2006]. Such a layered model approach, which better describes the "radar" properties of

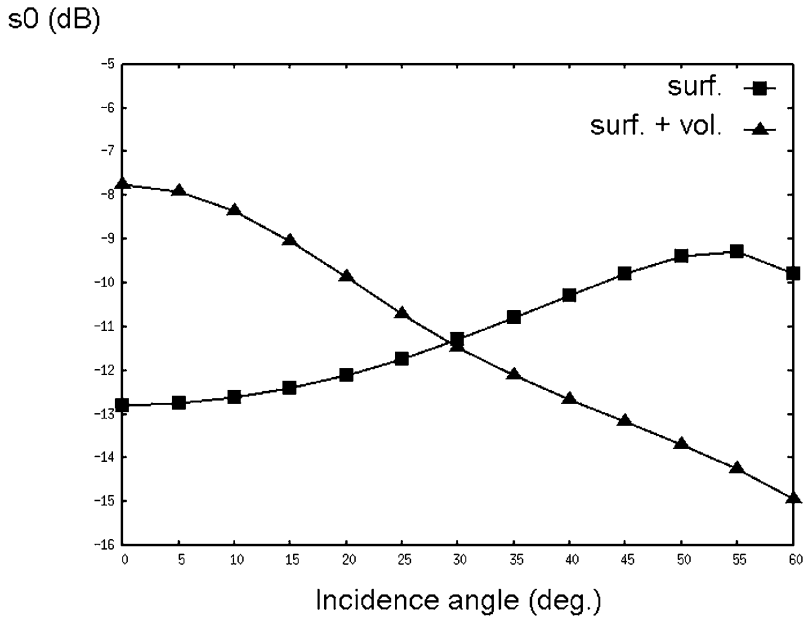

Figure 7. Computed backscattering power for a tholin-composed radar-dark spot with respect to the SAR incidence angle: surface scattering only model (squares) and surface plus volume scattering model (triangles).

Titan's surface [*Wye et al.*, 2006], should nevertheless be supported by future physical models of surface processes. Radar-dark spots, which are candidate hydrocarbon lakes, can be modeled with two scenarios: a rough tholin surface or a smoother one with some volume scattering. We show that the use of multi-incidence SAR data (higher incidence for radar-bright features and lower incidence for radar-dark spots) could help discriminate between the proposed interpretations.

[32] **Acknowledgments.** The authors are grateful to two anonymous reviewers for their critical and valuable comments on earlier versions of this manuscript.

References

Elachi, C., L. E. Roth, and G. G. Schaber (1984), Spaceborne radar subsurface imaging in hyperarid regions, *IEEE Trans. Geosci. Remote Sens.*, *22*, 383–388.

Elachi, C., et al. (2004), RADAR: The Cassini Titan radar mapper, *Space Sci. Rev.*, *115*, 71–110.

Elachi, C., et al. (2005), Cassini radar views the surface of Titan, *Science*, *308*, 970–974.

Fung, A. K. (1994), *Microwave Scattering and Emission Models and their Applications*, Artech House, Norwood, Mass.

Fung, A. K., and H. J. Eom (1981), Multiple scattering and depolarization by a randomly rough Kirchhoff surface, *IEEE Trans. Antennas Propag.*, *29*(3), 463–471.

Fung, A. K., Z. Li, and K. S. Chen (1992), Backscattering from a randomly rough dielectric surface, *IEEE Trans. Geosci. Remote Sens.*, *30*, 356–369.

Hallikainen, M., F. Ulaby, and T. Deventer (1987), Extinction behavior of dry snow in the 18- to 90-GHz range, *IEEE Trans. Geosci. Remote Sens.*, *25*, 737–745.

Lopes, R. M., et al. (2005), Cryovolcanic features on Titan's surface as revealed by the Cassini radar, *Proc. Lunar Planet. Sci. Conf. 36th*, abstract 1885.

Lorenz, R. D., et al. (2003), Cassini radar: Prospects for Titan surface investigations using the microwave radiometer, *Planet. Space Sci.*, *51*, 353–364.

Lorenz, R. D., et al. (2005), Titan's elusive lakes? Properties and context of dark spots in Cassini Ta radar data, *Proc. Lunar Planet. Sci. Conf. 36th*, abstract 1682.

Lunine, J. I. (1993), Does Titan have an ocean? A review of current understanding of Titan's surface, *Rev. Geophys.*, *31*, 133–150.

Ostro, S. J., et al. (1992), Europa, Ganymede and Callisto: New radar results from Arecibo and Goldstone, *J. Geophys. Res.*, *97*, 18,227–18,244.

Paganelli, F., et al. (2005), Channels and fan-like features on Titan surface imaged by the Cassini radar, *Proc. Lunar Planet. Sci. Conf. 36th*, abstract 2150.

Rignot, E. (1995), Backscatter model for the unusual radar properties of the Greenland Ice Sheet, *J. Geophys. Res.*, *100*, 9389–9400.

Rodriguez, S., et al. (2003), Impact of tholins present in Titan's atmosphere on the Cassini radar experiment, *Icarus*, *164*(1), 213–227.

Saunders, R. S., et al. (1992), The Magellan mission summary, *J. Geophys. Res.*, *97*, 13,067–13,090.

Sotin, C., et al. (2005), Release of volatiles from a possible cryovolcano from near-infrared imaging of Titan, *Nature*, *435*, 786–789.

Tobie, G., J. I. Lunine, and C. Sotin (2006), Episodic outgassing as the origin of atmospheric methane on Titan, *Nature*, *440*, 61–64.

Ulaby, F. T., R. K. Moore, and A. K. Fung (1982), *Microwave Remote Sensing: Active and Passive*, vol. 2, Artech House, Norwood, Mass.

Wye, L. C., H. A. Zebker, and R. D. Lorenz (2006), Modeling Titan's surface from Cassini radar's scatterometer and radiometer measurements, *Proc. Lunar Planet. Sci. Conf. 36th*, abstract 1473.

M. Crapeau and P. Paillou, UMR 5804, Observatoire Aquitain des Sciences de l'Univers, F-33270 Floirac, France. (philippe.paillou@obs.u-bordeaux1.fr)

C. Elachi and S. Wall, JPL, 4800 Oak Grove Drive, Pasadena, CA 91109, USA.

P. Encrenaz, Laboratorie d'Etude du Rayonnement et de la Matiére en Astrophysique, Observatoire de Paris, 61, avenue de l''observatoire, F-75014, Paris, France.